ACCOUNTS
of chemical research

Multiple Exciton Generation and Recombination in Carbon Nanotubes and Nanocrystals

YOSHIHIKO KANEMITSU
Institute for Chemical Research, Kyoto University, Uji, Kyoto 611-0011, Japan

RECEIVED ON JUNE 27, 2012

CONSPECTUS

Semiconducting nanomaterials such as single-walled carbon nanotubes (SWCNTs) and nanocrystals (NCs) exhibit unique size-dependent quantum properties. They have therefore attracted considerable attention from the viewpoints of fundamental physics and functional device applications. SWCNTs and NCs also provide an excellent new stage for experimental studies of many-body effects of electrons and excitons on optical processes in nanomaterials. In this Account, we discuss multiple exciton generation and recombination in SWCNTs and NCs for next-generation photovoltaics.

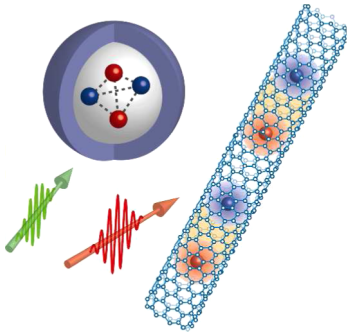

Strongly correlated ensembles of conduction-band electrons and valence-band holes in semiconductors are complex quantum systems that exhibit unique optical phenomena. In bulk crystals, the carrier recombination dynamics can be described by a simple model, which includes the nonradiative single-carrier trapping rate, the radiative two-carrier recombination rate, and the nonradiative three-carrier Auger recombination rate. The nonradiative Auger recombination rate determines the carrier recombination dynamics at high carrier density and depends on the spatial localization of carriers in two-dimensional quantum wells. The Auger recombination and multiple exciton generation rates can be advantageously manipulated by nanomaterials with designated energy structures. In addition, SWCNTs and NCs show quantized recombination dynamics of multiple excitons and carriers. In one-dimensional SWCNTs, excitons have large binding energies and are very stable at room temperature. The extremely rapid Auger recombination between excitons determines the photoluminescence (PL) intensity, the PL linewidth, and the PL lifetime. SWCNTs can undergo multiple exciton generation, while strong exciton–exciton interactions and complicated exciton structures affect the quantized Auger rate and the multiple exciton generation efficiency. Interestingly, in zero-dimensional NC quantum dots, quantized Auger recombination causes unique optical phenomena. The breakdown of the *k*-conversion rule and strong Coulomb interactions between carriers in NCs enhance Auger recombination rate and decrease the energy threshold for multiple exciton generation. We discuss this impact of the *k*-conservation rule on two-carrier radiative recombination and the three-carrier Auger recombination processes in indirect-gap semiconductor Si NCs. In NCs and SWCNTs, multiple exciton generation competes with Auger recombination, surface trapping of excitons, and cooling of hot electrons or excitons. In addition, we explore heterostructured NCs and impurity-doped NCs in the context of the optimization of charge carrier extraction from excitons in NCs.

1. Introduction

Over the past four decades, the dynamics of high-density electron–hole systems in photoexcited semiconductors have been extensively studied both theoretically and experimentally, and achieving a deep understanding of these systems has been a long-standing, central issue in condensed matter physics.[1] Ensembles of the conduction-band electrons and valence-band holes in semiconductors are complex systems that exhibit strong Coulomb interactions. Unique optical processes appear in these systems, owing to the presence of excitons, trions, biexcitons (excitonic molecules), bound exciton complexes, electron–hole liquids, and electron–hole plasmas. Semiconducting nanocrystals (NCs) and single-walled carbon nanotubes (SWCNTs) currently provide an excellent stage for experimental studies of the many-body effects of electrons and excitons on optical processes in nanoscale materials.[2,3] They also exhibit unique nonlinear optical properties that give them an advantage over semiconductor bulk crystals for photonic applications. Quantum confinement of excitons and electrons in NCs and SWCNTs enhances dynamical exciton–exciton and electron–electron interactions, leading to many-body processes such as quantized

Published on the Web 02/19/2013 www.pubs.acs.org/accounts
10.1021/ar300269z

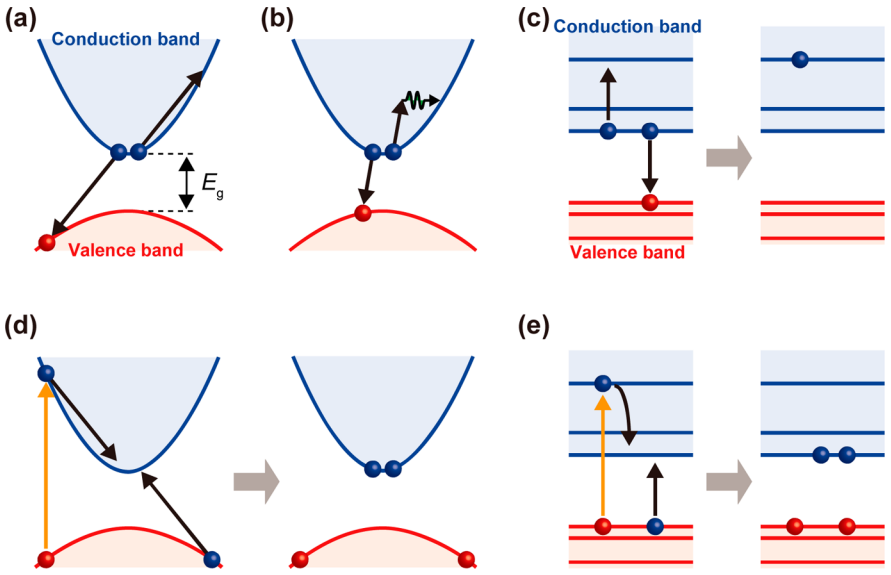

FIGURE 1. AR and MEG in bulk crystals (a, b, d) and in nanocrystals (c, e). AR reduces the number of e−h pairs and produces hot electrons or holes (a, b, c). No-phonon and phonon-assisted AR are illustrated in panels a and b, respectively. In MEG (d, e), the excess energy of e−h pairs is used to generate new e−h pairs. In bulk crystals, the *k*-conservation rule dictates the AR and MEG rates. In nanocrystals, energy conservation determines the AR and MEG rates.

Auger recombination (AR) and multiple exciton generation [(MEG) or carrier multiplication (CM)].[2−4]

In MEG, a single photon creates two or more excitons in semiconductors. This MEG process has attracted considerable interest for high-performance solar cell applications. It was proposed that MEG efficiencies are enhanced in NCs.[5] Since the first experimental demonstration in 2004,[6] MEG has been observed in a variety of NCs.[4,6−9] Many researchers have attempted to minimize the artifacts from photoionized or photocharged NCs by flowing or stirring the NC solution,[8,9] and the improved optical measurements showed that the MEG efficiencies in PbSe NCs are smaller than the initially reported values,[8−10] but are comparable to or smaller than those in bulk crystals when measured for the same excitation energy.[8,10,11] It is not clear whether MEG in NCs is effective in the high photon-flux region in the solar spectrum. On the other hand, in NC-based device structures such as photodetectors and photovoltaic cells, photocurrent enhancement by MEG has been demonstrated.[12,13] Thus, the MEG process and increased band gap in NCs are believed to play an essential role in next-generation photovoltaics based on nanomaterials for exceeding the Shockley−Queisser limit in single junction solar cells.[14] However, the MEG mechanism in NCs and the merits of NC solar cells are currently under discussion. Here, we summarize our recent spectroscopic studies of the dynamic properties of multiexcitons in bulk crystals, two-dimensional (2D) quantum wells, one-dimensional (1D) SWCNTs, and zero-dimensional (0D) NCs. Studies on multiexciton dynamics in these various types of semiconductor nanostructures provide further insight into the AR and MEG processes that underlie the application of NCs and SWCNTs to photovoltaics.

2. Three-Carrier Interactions in Semiconductors

We begin with a brief discussion of the simple three-carrier AR and MEG processes in semiconductors. Figure 1 illustrates the three-carrier AR (Figure 1a,b,c) and MEG in semiconductors (Figure 1d,e); in this figure E_g represents the band-gap energy. In AR, the electron−hole (e−h) recombination energy is transferred to another electron or hole. The numbers of electrons and holes decrease, and hot electrons are produced. In the high-density carrier region, nonradiative AR dominates the carrier density and carrier lifetime, thereby determining the optical device performance.

In bulk crystals, the momentum conservation rule, that is, the *k*-conservation rule, dictates the three-carrier AR rate because an electron or a hole needs to gain both the energy and the momentum of the recombined e−h pairs (Figure 1a). Thus, the AR rate depends exponentially on the band-gap energy and is sensitive to the temperature.[15] Another process is a phonon-assisted mechanism. Phonon-assisted AR shows a weak temperature dependence.[16] Phonon scattering enables AR transitions to a final state with a large density (Figure 1b). The AR rate depends on the band structure of semiconductors (e.g., whether direct-gap or indirect-gap

semiconductors).[15,16] In 0D NCs, the breakdown of the *k*-conservation rule affects the AR rates (Figure 1c). The quantization of AR rates occurs in NCs,[17] as discussed in section 5.

In the MEG process, on the other hand, the excess energy of photocreated "hot" electrons or excitons is used to generate new e−h pairs or excitons (Figure 1d). Here, we discuss CM in the case of bulk crystals, because charge carrier generation efficiency has been discussed using photocurrent measurements for bulk crystals.[18,19] From Figure 1, the MEG and CM processes for NCs and bulk crystals can be regarded as the inverse of the AR process. In bulk crystals, CM occurs through impact ionization (II).[18,19] When we assume single parabolic bands for the conduction and valence bands and the same effective masses for elections and holes, the CM threshold is $4E_g$. The relaxation of the *k*-conservation rule and a large asymmetrical electron/hole mass ratio reduce the energy threshold for MEG in NCs (e.g., Figure 1e).[20]

Many papers reported high MEG efficiencies and low MEG thresholds normalized by the band-gap energies in NCs.[4,9] Several models have been proposed for these findings: for instance, coherent superposition of single- and multiexciton states,[7] and second-order coupling with virtual single-exciton states.[21] Theoretical papers suggested that many data can be explained by the II model,[22,23] which is the favored model. Large difference between the MEG and AR rates is described according to the density of final states for these processes, that is, the densities of states of single excitons and biexcitons.[22] The detailed MEG mechanism remains unclear.[24,25]

We need to consider competition between the MEG and the relaxation processes such as AR, radiative recombination, and phonon-assisted cooling. Many processes affect the MEG efficiency. NCs have advantages and disadvantages for MEG, compared with the case of the parent bulk crystal. It is expected that the MEG efficiencies in NCs are enhanced, owing to slow relaxation of hot carriers and strong Coulomb interactions.[5,6] The stronger Coulomb interaction results from spatial overlap between electrons and holes and reduced dielectric screening at the NC surface.[26] The discrete states in NCs may slow the electron−phonon relaxation rate near the band edge.[27] However, slow relaxation of hot carriers is not expected in high-energy states because of the continuous high density of states in the high-energy region.[11] In contrast, the decrease of the MEG efficiency may be caused by the reduced density of states in NCs[11] and hot-carrier trapping at NC surface states because of their large surface-to-volume ratios.[28] For these reasons, the MEG and AR processes are complicated in NCs. In the following sections, we discuss AR and MEG in bulk crystals and in nanomaterials. Deep understanding of the AR process is essential for assessment of the MEG efficiency of solar cell materials and photocurrent enhancement in nanostructure-based intermediate-band solar cells.[29]

3. Bulk Crystals, Quantum Wells, and Superlattices

In bulk crystals, a large number of carriers exist in the large crystal volumes.Thus, the carrier recombination dynamics can be described by the continuous change in the carrier density in bulk crystals. The recombination processes of electrons and holes in semiconductors are usually expressed as a power series of the electron density, *n*, and hole density, *p*. Under photoexcitation of intrinsic semiconductors, the numbers of electrons and holes are considered to be equal: $n = p$. The rate equation for the photocarriers can therefore be written simply as follows:[15,30]

$$\frac{dn}{dt} = -An - Bn^2 - Cn^3 \quad (1)$$

An represents the nonradiative single-carrier trapping rate at the defects. Bn^2 is the two-carrier radiative recombination rate, and Cn^3 is the nonradiative AR rate, including three-carrier, electron−hole−electron, and electron−hole−hole processes.

Here, we show the importance of AR even in bulk crystals. We determined the PL intensity and PL lifetime of the perovskite semiconductor $SrTiO_3$ as a function of the photocarrier density and the chemically doped electron density. Because of its high dielectric constant, only band-to-band recombination appears even at low temperatures (no exciton effects).[30−32] In Figure 2a, we summarize the excitation intensity dependence of the PL decay time and PL intensity in undoped $SrTiO_3$ at room temperature.[30] Broad PL appears at around 2.9 eV, and PL decay curves were measured using a streak camera. Since the PL efficiency is poor, the Bn^2 term in eq 1 is negligibly small. Under strong photoexcitation, the PL decay time decreases, and the PL intensity gets saturated. These behaviors can be explained by the preceding simple rate equation, eq 1.

In electron-doped samples, La-doped $SrTiO_3$ and Nb-doped $SrTiO_3$, the PL properties depend on the doped electron density. In Figure 2b, the PL decay time and PL intensity of doped samples are summarized as a function of the doped electron density.[30] The photocarrier density is much lower than the chemically doped electron density.

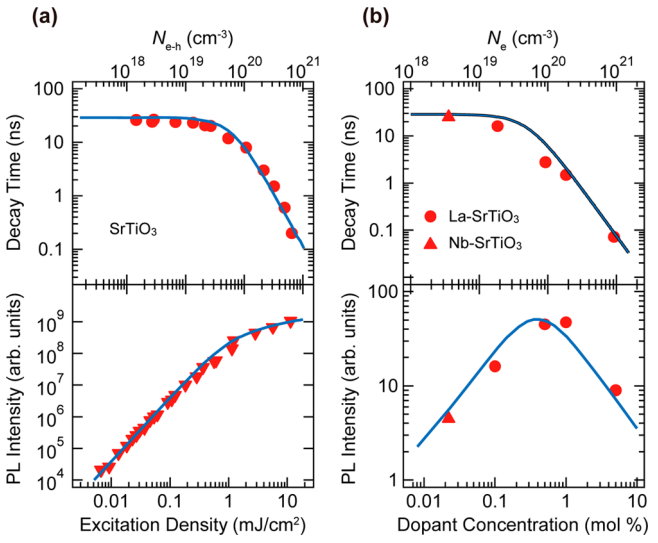

FIGURE 2. (a) Excitation laser intensity dependence of the PL decay time and PL intensity in undoped $SrTiO_3$ at room temperature. (b) PL decay time and PL intensity of electron-doped $SrTiO_3$ as a function of dopant concentration. Broad PL at around 2.9 eV is obtained under 3.49 eV, 150 fs laser excitation in undoped and doped samples. Solid curves represent the results of calculations using the simple rate equation. Images reproduced from ref 30. Copyright 2008 by American Physical Society.

In the high-electron-density region, nonradiative AR between doped electrons and photocreated e−h pairs determines the PL properties. The numerical calculations based on the rate equation are plotted as solid curves.[30] Surprisingly, in both undoped and electron-doped $SrTiO_3$, the PL dynamics are explained well by the simple rate equation. We obtained $A = 1.7 \times 10^7\ s^{-1}$ and $C = 1.2 \times 10^{-32}\ cm^6\ s^{-1}$ as the best-fit parameters. These PL data were also confirmed by femtosecond transient absorption (TA) spectroscopy.[33] In the TA experiment, we can measure transient carrier-induced absorption changes and evaluate temporal changes in carrier density. Our findings clearly show that the three-body AR process determines the optical properties of highly photoexcited and heavily doped semiconductors.

To manipulate the AR rate in semiconductors, we studied the PL spectra and dynamics of $Si_{1-x}Ge_x$/Si single quantum wells, coupled double quantum wells, and superlattice structures at low temperatures.[34,35] It was found that the spatial localization of carriers enhances the AR rate in these Si-based nanostructures.[34] Controlling the spatial extension of the carriers is important for manipulation of the AR rate in semiconductors. We anticipate that quantum heterostructures with the designed energy band structures have advantages for controlling the AR and MEG rates, which is discussed in the following section.

4. Carbon Nanotubes

The preceding section showed that AR is the dominant recombination process at high carrier density. Because nanomaterials have small volumes, the carrier density is extremely high even when two pairs are excited. Thus, the AR and MEG rates should be strongly enhanced in nanomaterials. In addition, we must consider the quantized character of number of e−h pairs in 1D SWCNTs and 0D NCs: Quantized recombination dynamics of multiple excitons and carriers can be described by a set of discrete time constants.[17,36,37] In this section, we discuss the AR and MEG processes in a typical 1D material, SWCNTs. In SWCNTs, excitons with huge binding energies are stable at room temperature.[38] The 1D exciton determines the optical properties of SWCNTs.[3,39] The AR process in SWCNTs is exciton−exciton collision.[37,40] The multiexciton dynamics in SWCNTs were studied using single-nanotube spectroscopy and pump-and-probe spectroscopy.

For single-nanotube spectroscopy, we fabricated isolated SWCNT samples on patterned Si substrates using chemical vapor deposition. We obtained a very sharp PL spectrum for a single SWCNT suspended on the substrate. The spectral shape is approximately described by a single Lorentzian function, and the PL energy depends on the diameter, as shown in Figure 3a. The very sharp PL line of a single SWCNT yields considerable information on the 1D free exciton properties.[41] The PL intensity of a single (11,4) SWCNT becomes saturated at high-intensity excitation, as shown in Figure 3b.[42] Simultaneously, the spectral linewidth of a single SWCNT increases with increasing excitation (Figure 3c).[42] Under strong photoexcitation, broadening of the homogeneous linewidth and saturation of the PL intensity occur due to the nonradiative Auger process. When two or more excitons are created in a SWCNT, a fast recombination between excitons occurs. The numerical calculation fittings in Figure 3b,c show that AR between excitons occurs.

To examine the exciton decay dynamics, we measured the temporal change in the exciton number in (6,5) SWCNT ensemble samples by femtosecond TA spectroscopy. Some transient bleaching signals at the lowest E_{11} exciton energy under 1.55 eV, 150 fs excitation are shown in Figure 3d.[43] As the excitation intensity increases, a rapid decay component appears in the picosecond time region because of nonradiative Auger processes involving excitons. In SWCNTs, rapid AR determines the exciton dynamics because of strong Coulomb interactions between excitons confined in 1D structures.

In SWCNTs, spatially confined excitons in 1D structures enhance the exciton−exciton interactions, leading to

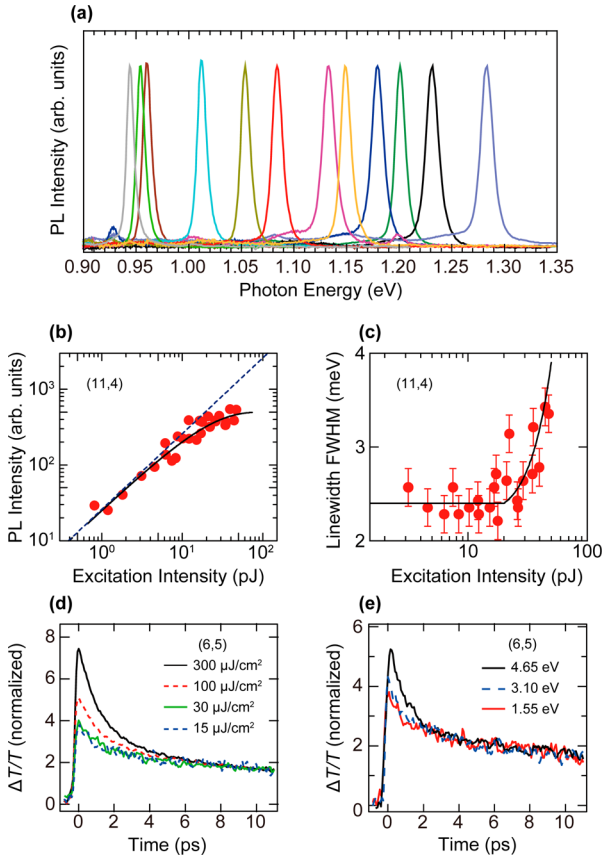

FIGURE 3. (a) PL spectra of single SWCNTs. (b) PL linewidth and (c) PL intensity of a single (11,4) SWCNT as a function of the 1.72 eV, 150 fs excitation laser intensity at 30 K. (d) Transient absorption dynamics of (6,5) SWCNT ensembles under 1.55 eV, 150 fs excitation at room temperature under different intensities. Transient absorption decay curves are normalized by the long decay component at 10 ps. The exciton density was monitored at the lowest E_{11} exciton energy of 1.22 eV. (e) Normalized transient absorption decays of (6,5) SWCNT ensembles under the weak excitation regime with different excitation photon energies. Panels b and c were reproduced from ref 42. Copyright 2008 by American Physical Society. Panels d and e reprinted with permission from ref 43. Copyright 2008 American Institute of Physics.

efficient MEG processes. Under weak excitation, the TA decay curve monitored at the E_{11} exciton energy depends on the excitation wavelength, but not on the excitation intensity (Figure 3e).[43] When the photon energy is three times larger than the E_{11} exciton energy, fast decay appears through the AR process, indicating that MEG occurs at short wavelengths. The MEG efficiency is estimated to be about 1.3 at about $3.8E_g$ energy. A low MEG threshold was also reported in SWCNTs.[44] Strong interactions between excitons and multiexciton recombination processes are expected to create new optical functionalities in SWNTs.

Theoretical studies of SWCNTs have predicted that the two degenerate valleys create multiple exciton states.[45] Only the odd-parity exciton with spin singlet and zero

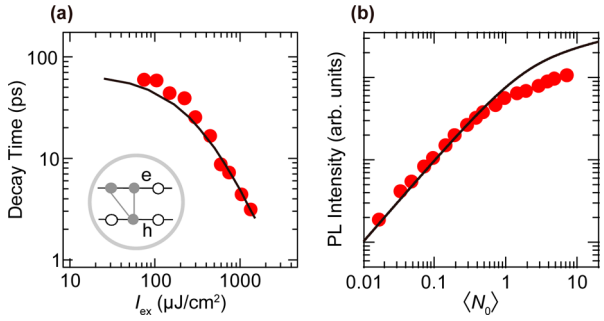

FIGURE 4. (a) Biexciton AR decay time in CdSe NCs as a function of the 3.1 eV, 150 fs excitation laser intensity at room temperature. Solid curve shows the calculated results using the quantized AR model with three-carrier collisions as shown in the inset. (b) Mn^{2+}-related PL intensity in 2 mol % Mn^{2+}-doped CdS NCs under 3.1 eV, 150 fs laser excitation. Solid curve shows the calculated PL intensity assuming energy transfer to Mn^{2+} ions and AR. Panel a reproduced with permission from ref 49. Copyright 2009 Physical Society of Japan. Panel b reproduced with permission from ref 53. Copyright 2010 Physical Society of Japan.

angular momentum (called the bright exciton) can recombine radiatively; all the other exciton states are all dipole-forbidden dark ones.[45] We experimentally determined the energy differences between the bright and even-parity dark excitons, between the bright and triplet excitons, and between the bright excitons and trions in SWCNTs.[46] The underlying dark excitons and trions strongly affect the observation of the AR and MEG processes of bright excitons. A detailed understanding of exciton and trion dynamics is needed to clarify the recombination mechanism[47] and control the AR and MEG processes in SWCNTs.

5. Nanocrystals

The multiexciton dynamics in a variety of NCs have been extensively studied by many groups. In NCs, a discrete change in the number of carriers, N, is observed, in contrast to bulk crystals (continuous change in the carrier density). The three-body AR rate is described by a simple equation,[48,49]

$$\tau_N^{-1} = \frac{N^2(N-1)}{2}\gamma_{\text{Auger}} \qquad (2)$$

where γ_{Auger} is a constant. The quantized AR rates cause unique optical processes such as PL blinking.[50−52] In this section, we present our study of the AR dynamics in NCs using femtosecond pump−probe spectroscopy based on intraband transitions and the lowest exciton bleaching. Figure 4a shows the Auger decay time of CdSe NCs (2.07 eV exciton energy) as a function of the femtosecond excitation intensity, I_{ex},[49] where Auger decay time was

monitored at the intraband transition of 0.84 eV. The decay time decreases rapidly as the excitation intensity increases. Here, we considered a three-carrier collision process of carriers in the N e−h pair state (or N-exciton state), as illustrated in the inset, and assumed a Poisson distribution of the initial e−h pair number in a given NC in the analysis. Our experimental results are reproduced by the quantized AR model with three-carrier collisions.

For controlling the AR rate, we fabricated functional-impurity-doped NCs and studied their optical properties. In Mn-doped NC samples, the Mn^{2+} PL intensity depends on the excitation intensity and is determined by competition between the energy transfer from NCs into Mn^{2+} ions and the recombination of multiexcitons in NCs. We compared the TA bleaching of the lowest-energy 1S state in CdS NCs with that in Mn-doped CdS NCs and discussed the impact of the AR process on recombination.[53] At low excitation intensities, energy transfer from e−h pairs in CdS NCs to Mn^{2+} ions dominates the single e−h pair recombination. At high excitation intensities, the decay of multicarriers is determined by nonradiative AR in NCs. This trend is also confirmed by the excitation intensity dependence of the Mn^{2+} PL properties.

Figure 4b shows the Mn^{2+} PL intensity as a function of the average number of initially created e−h pairs, $\langle N_0 \rangle$.[53] At extremely high density, the nonradiative AR rate in the host NCs is larger than the energy transfer rate from multiple e−h pairs to Mn^{2+} ions. At intermediate density, the AR rate is comparable to the energy transfer rate. The N e−h pair state decays sequentially to the $(N-1)$ e−h pair state and finally to the single e−h pair state. Then, the total number of Mn^{2+} ions excited by sequential energy transfer from the initially photocreated e−h pair state is calculated (solid curve in Figure 4b). A simple calculation can explain the experimental results.[53] Recently, the AR rate in M^{2+}-doped NCs is controlled using an electrochemical carrier doping technique, and the Auger processes are also discussed.[54] Because strong interactions between confined carriers and impurities cause unique optical and magnetic properties, impurity-doped NCs may also open a new way to control multiexciton processes. We expect that doping of shallow donors as well as localized impurities into NCs makes it possible to modify the MEG rate.

The quantized AR process is the dominant type of recombination in NCs.[17,48] However, the detailed mechanism of the AR process remains unclear, for example, the temperature dependence of measurements of the MEG and AR

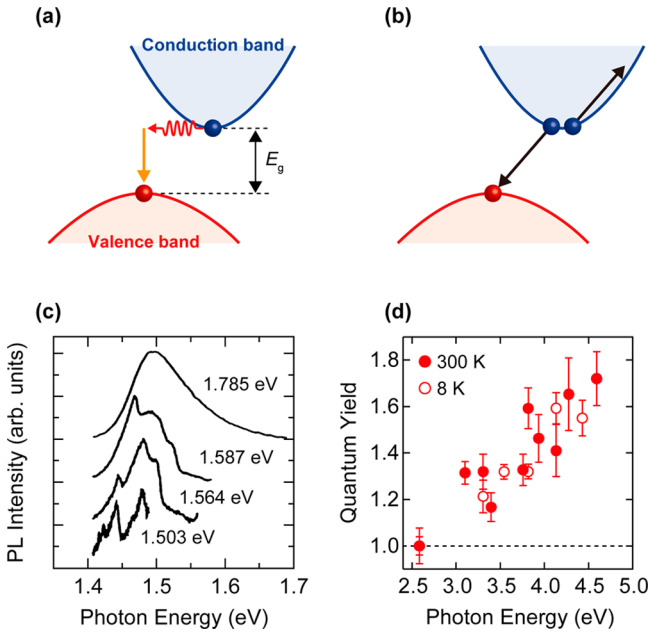

FIGURE 5. (a) Radiative recombination and (b) three-carrier AR processes in indirect-gap semiconductors. (c) Resonantly excited PL spectra of porous silicon at 7 K. Excitation photon energies are shown in the figure. (d) MEG efficiencies in Si NCs embedded in SiO_2 matrices at 8 and 300 K under wavelength-tunable 150 fs laser excitation. Panel c reproduced from ref 60. Copyright 1998 American Physical Society.

rates.[55,56] Challenges still remain regarding experimental evidence of the breakdown of the k-conservation rule in optical processes in NCs.[56,57] Experimental studies of indirect-gap semiconductors such as Si crystals give hints for understanding the role of momentum conservation in recombination processes.[56] PL and AR processes in indirect-gap semiconductors are illustrated in Figure 5a,b.

In Si bulk crystals, the top of the valence band is located at the Γ point, and the bottom of the conduction band is located near the X point. PL in Si bulk crystals is caused by TA(Δ)- and TO(Δ)-phonon-assisted radiative recombination, where TA(Δ) and TO(Δ) are transverse acoustic and transverse optical phonons, respectively, at the conduction-band-minimum Δ point.[58,59] Figure 5c shows PL spectra of porous Si, one type of Si NCs, under different excitation energies at 7 K.[60] Resonant excitation at energies within the broad PL band produces fine structure in the spectrum. These step and peak structures in the resonantly excited PL spectra can be explained by momentum-conserving phonon-assisted luminescence processes [TA(Δ), TO(Δ), TA(Δ)+TO(Δ), or 2TO(Δ)].[60] PL studies have shown that in Si NCs, the optical transitions are blue-shifted, and the oscillator strengths of the no-phonon and phonon-assisted processes are modified.[59,61] In Si NCs, the absorption and emission of momentum-conserving phonons are needed during light

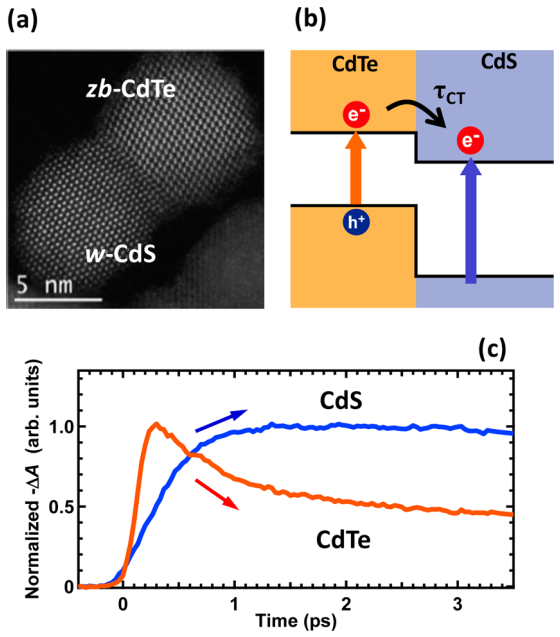

FIGURE 6. (a) Atomic-resolution high-angle annular dark-field scanning transmission electron microscopy image of a single heterodimer NC consisting of wurtzite CdS (w-CdS) and zinc blende CdTe (zb-CdTe). (b) Energy diagram of the CdS/CdTe heterodimer, (c) Kinetics of CdTe (probed at 1.82 eV) and CdS state-filling signals (probed at 2.53 eV) under 2.07 eV, 150 fs laser excitation at room temperature. Panels a and c reproduced from ref 64. Copyright 2011 American Chemical Society.

absorption and emission. The next question is whether the conserving phonon is needed for AR and MEG.

AR is based on three-carrier collisions, whereas PL is related to e–h recombination. In AR, the recombination energy of e–h pairs is transferred to another electron or hole, where the momentum of the recombined e–h pair is not required to be zero. The no-phonon and phonon-assisted Auger transitions are possible even in bulk crystals,[15,16] as illustrated in Figure 5b (also see Figure 1a). No temperature dependence of the AR rate was observed in Si NCs,[56] whereas Si bulk crystals exhibit a temperature dependence.[62] In addition, the MEG efficiency of Si NCs (1.46 eV band gap) is also independent of temperature (Figure 5d), where the MEG efficiency was evaluated using femtosecond intraband pump–probe spectroscopy and the analytical procedure in ref 63. Details will be discussed elsewhere. The MEG threshold appears at around $2E_g$ in NCs and is below about $4E_g$ in bulk crystals. Similar results have been reported in Si NC solutions.[63] These MEG efficiencies in NCs solids and solutions (ref 63) are higher than those in bulk crystals in ref 19. Si NCs show the temperature independence of the AR rate and MEG efficiency and the low-energy MEG threshold, indicating the breakdown of the *k*-selection rule in MEG.

The MEG process competes with the AR process and phonon-assisted carrier cooling. For photovoltaics, we need to reduce the AR rate and extract charge carriers from NCs. In terms of the structure-specific properties, type-II heterostructures may allow spatial carrier separation. Here, we describe our recent attempt at charge carrier extraction using the band-edge alignment between CdS and CdTe in a heterodimer (Figure 6a), in which photoexcited electrons and holes are confined in the CdS and CdTe components, respectively.[64] The pump pulse was tuned to photoexcite only the CdTe phases, as illustrated in Figure 6b. The two bleaching peaks are due to the CdS and CdTe exciton transitions by state filling. State filling in CdS and slow rise of the CdS bleaching should be induced by electron injection from the CdTe phase to the CdS phase (Figure 6c). The efficient spatial charge separation was further supported by considerable quenching of the CdS emission in the PL spectrum of the CdS/CdTe heterodimers. These results strongly demonstrate that the type-II band-aligned heterointerface effectively produces photoexcited spatial charge separation.[64] Heterostructured NCs including rods and tetrapods have practical potentials for photovoltaics.

6. Concluding Remarks and Perspectives

We discussed the multiexciton generation and recombination dynamics in bulk crystals, 2D quantum wells, 1D nanotubes, and 0D nanocrystals. SWCNTs and NCs show quantized recombination dynamics of multiple excitons and carriers. We noted that strong exciton–exciton interactions and complicated exciton structures affect the AR and MEG rates, on the basis of observations of extremely fast AR processes between stable excitons in SWCNTs. In NCs, the AR and MEG rates are enhanced by quantum confinement of carriers and the breakdown of the *k*-conservation rule in three-carrier scattering processes. We discussed the role of phonons in two-body radiative recombination and the three-carrier AR and MEG processes in indirect-gap Si NCs.

Moreover, we pointed out the need to develop new heterostructures for effective carrier extraction for practical solar cells, because of the trade-off relationship between the spatial confinement of carriers and carrier transport.[65] We presented the rapid charge separation in heterointerfaces with asymmetrical potential profiles. Surface modification of NCs is also essential for the MEG and charge extraction processes.[65,66] Moreover, NCs and SWCNTs can become building blocks for unique heterostructures. Their optical properties are sensitive to the surrounding environment. For example, dramatic changes in their optical properties are

obtained by controlling the energy transfer through exciton−plasmon interactions in close-packed heterostructures of semiconductor and metal NCs and energy transfer at heterostructures.[67] Doping of carriers and functional impurities into NCs and SWCNTs and p−n junctions in NCs and SWCNTs reveals new optical and electrical phenomena for photovoltaics. Dynamical interactions of multiexcitons, exciton complexes, and multicarriers provide an excellent opportunity for the development of innovative new devices with functionalities beyond those of the current devices and for fundamental physics based on quantum ensembles with strong Coulomb correlations.

The author would like to thank many colleagues and his graduate students for their contributions and discussions. In particular, M. Okano, S. Taguchi, R. Matsunaga, K. Ueda, K. Matsuda, and T. Teranishi deserve mention here. Part of this work was supported by KAKENHI (No. 20104006), JST-CREST, and The Sumitomo Electric Industries Group CSR Foundation.

BIOGRAPHICAL INFORMATION

Yoshihiko Kanemitsu is a Professor of Institute for Chemical Research, Kyoto University. He received his Ph.D. in 1986 from The University of Tokyo. Currently, his interest is focused on optical properties and functionalities of exciton complexes and high-density electron−hole pairs in semiconductor nanostructures.

FOOTNOTES

The author declares no competing financial interest.

REFERENCES

1 Chemla, D. S.; Shah, J. Many-body and correlation effects in semiconductors. *Nature* **2001**, *411*, 549–557.

2 Klimov, V. I. Spectral and dynamical properties of multiexcitons in semiconductor nanocrystals. *Annu. Rev. Phys. Chem.* **2007**, *58*, 635–673.

3 Kanemitsu, Y. Excitons in semiconducting carbon nanotubes: Diameter-dependent photoluminescence spectra. *Phys. Chem. Chem. Phys.* **2011**, *13*, 14879–14888.

4 Nozik, A. J.; Beard, M. C.; Luther, J. M.; Law, M.; Ellingson, R. J.; Johnson, J. C. Semiconductor quantum dots and quantum dot arrays and applications of multiple exciton generation to third-generation photovoltaic solar cells. *Chem. Rev.* **2010**, *110*, 6873–6890.

5 Nozik, A. J. Quantum dot solar cells. *Physica E* **2002**, *14*, 115–120.

6 Schaller, R .D.; Klimov, V. I. High efficiency carrier multiplication in PbSe nanocrystals: Implications for solar energy conversion. *Phys. Rev. Lett.* **2004**, *92*, No. 186601.

7 Ellingson, R. J.; Beard, M. C.; Johnson, J. C.; Yu, P.; Micic, O. I.; Nozik, A. J.; Shabaev, A.; Efros, Al. L. Highly efficient multiple exciton generation in colloidal PbSe and PbS quantum dots. *Nano Lett.* **2005**, *5*, 865–871.

8 McGuire, J. A; Sykora, M.; Joo, J.; Pietryga, J. M.; Klimov, V. I. Apparent versus true carrier multiplication yields in semiconductor nanocrystals. *Nano Lett.* **2010**, *10*, 2049–2057.

9 Beard, M. C. Multiple exciton generation in semiconductor quantum dots. *J. Phys. Chem. Lett.* **2011**, *2*, 1282–1288.

10 Nair, G.; Chang, L. Y.; Geyer, S. M.; Bawendi, M. G. Perspective on the prospects of a carrier multiplication nanocrystal solar cell. *Nano Lett.* **2011**, *11*, 2145–2151.

11 Pijpers, J. J. H.; Ulbricht, R.; Tielrooij, K. J.; Osherov, A.; Golan, Y.; Delerue, C.; Allan, G.; Bonn, M. Assessment of carrier-multiplication efficiency in bulk PbSe and PbS. *Nat. Phys.* **2009**, *5*, 811–814.

12 Sukhovatkin, V.; Hinds, S.; Brzozowski, L.; Sargent, E. H. Colloidal quantum-dot photodetectors exploiting multiexciton generation. *Science* **2009**, *324*, 1542–1544.

13 Semonin, O. E.; Luther, J. M.; Choi, S.; Chen, H. Y.; Gao, J.; Nozik, A. J.; Beard, M. C. Peak external photocurrent quantum efficiency exceeding 100% via MEG in a quantum dot solar cell. *Science* **2011**, *334*, 1530–1533.

14 Shockley, W.; Queisser, H. J. Detailed balance limit of efficiency of p-n junction solar cells. *J. Appl. Phys.* **1961**, *32*, 510–519.

15 Landsberg, P. T *Recombination in Semiconductors*; Cambridge University Press: New York, 1991.

16 Haug, A. Band-to-band Auger recombination in semiconductors. *J. Phys. Chem. Sol.* **1988**, *49*, 599–605.

17 Klimov, V. I.; Mikhailovsky, A. A.; McBranch, D. W.; Leatherdale, C. A.; Bawendi, M. G. Quantization of multiparticle Auger rates in semiconductor quantum dots. *Science* **2000**, *287*, 1011–1013.

18 Werner, J. H.; Kolodinski, S.; Queisser, H. J. New optimization principles and efficiency limits for semiconductor solar cells. *Phys. Rev. Lett.* **1994**, *72*, 3851–3854.

19 Wolf, M.; Brendel, R.; Werner, J. H.; Queisser, H. J. Solar cell efficiency and carrier multiplication in $Si_{1-x}Ge_x$ alloys. *J. Appl. Phys.* **1998**, *83*, 4213–4221.

20 Schaller, R. D.; Pietryga, J. M.; Klimov, V. I. Carrier multiplication in InAs nanocrystal quantum dots with an onset defined by the energy conservation limit. *Nano Lett.* **2007**, *7*, 3469–3476.

21 Schaller, R. D.; Agranovich, V. M.; Klimov, V. I. High-efficiency carrier multiplication through direct photogeneration of multi-excitons via virtual single-exciton. *Nat. Phys.* **2005**, *1*, 189–194.

22 Franceschetti, A.; An, J. M.; Zunger, A. Impact ionization can explain carrier multiplication in PbSe quantum dots. *Nano Lett* **2006**, *6*, 2191–2195.

23 Delerue, C.; Allan, G.; Pijpers, J. J. H.; Bonn, M. Carrier multiplication in bulk and nanocrystalline semiconductors: Mechanism, efficiency, and interest for solar cells. *Phys. Rev. B.* **2010**, *81*, No. 125306.

24 Witzel, W. M.; Shabaev, A.; Hellberg, C. S.; Jacobs, V. L.; Efros, Al. L. Quantum simulation of multiple-exciton generation in a nanocrystal by a single photon. *Phys. Rev. Lett.* **2010**, *105*, No. 137401.

25 Velizhanin, K. A.; Piryatinski, A. Numerical study of carrier multiplication pathways in photoexcited nanocrystal and bulk forms of PbSe. *Phys. Rev. Lett.* **2011**, *106*, No. 207401.

26 Takagahara, T. Effects of dielectric confinement and electron-hole exchange interaction on excitonic states in semiconductor quantum dots. *Phys. Rev. B* **1993**, *47*, 4569–4584.

27 Pandey, A.; Guyot-Sionnest, P. Slow electron cooling in colloidal quantum dots. *Science* **2008**, *322*, 929–932.

28 Taguchi, S.; Saruyama, M.; Teranishi, T.; Kanemitsu, Y. Quantized Auger recombination of biexcitons in CdSe nanorods studied by time-resolved photoluminescence and transient-absorption spectroscopy. *Phys. Rev. B* **2011**, *83*, No. 155324.

29 Tex, D.; Kamiya, I.; Kanemitsu, Y. Efficient upconverted photocurrent through Auger process in disk-like InAs quantum structures for intermediate-band solar cells. Unpublished work, 2012.

30 Yasuda, H.; Kanemitsu, Y. Dynamics of nonlinear blue photoluminescence and Auger recombination in $SrTiO_3$. *Phys. Rev. B* **2008**, *77*, No. 193202.

31 Yamada, Y.; Yasuda, H.; Tayagaki, T.; Kanemitsu, Y. Temperature dependence of photoluminescence spectra of nondoped and electron-doped $SrTiO_3$: Crossover from Auger recombination to single-carrier trapping. *Phys. Rev. Lett.* **2009**, *102*, No. 247401.

32 Yamada, Y.; Kanemitsu, Y. Band-to-band photoluminescence in $SrTiO_3$. *Phys. Rev. B* **2010**, *82*, No. 121103(R).

33 Yamada, Y.; Yasuda, H.; Tayagaki, T.; Kanemitsu, Y. Photocarrier recombination dynamics in highly excited $SrTiO_3$ studied by transient absorption and photoluminescence spectroscopy. *Appl. Phys. Lett.* **2009**, *95*, No. 121112.

34 Tayagaki, T.; Fukatsu, S.; Kanemitsu, Y. Photoluminescence dynamics and reduced Auger recombination in $Si_{1-x}Ge_x$/Si superlattices under high-density photoexcitation. *Phys. Rev. B.* **2009**, *79*, No. 041301(R).

35 Tayagaki, T.; Fukatsu, S.; Kanemitsu, Y. Control of Auger recombination rate in $Si_{1-x}Ge_x$/Si heterostructures. *J. Phys. Soc. Jpn.* **2010**, *79*, No. 013701.

36 Htoon, H.; Hollingsworth, J. A.; Dickerson, R.; Klimov, V. I. Effect of zero- to one-dimensional transformation on multiparticle Auger recombination in semiconductor quantum rods. *Phys. Rev. Lett.* **2003**, *91*, No. 227401.

37 Wang, F.; Dukovic, G.; Knoesel, E.; Brus, L. E.; Heinz, T. F. Observation of rapid Auger recombination in optically excited semiconducting carbon nanotubes. *Phys. Rev. B* **2004**, *70*, No. 241403(R).

38 Wang, F.; Dukovic, G.; Brus, L. E.; Heinz, T. F. The optical resonances in carbon nanotubes arise from excitons. *Science* **2005**, *308*, 838–841.

39 Dresselhaus, M. S.; Dresselhaus, G.; Saito, R.; Jorio, A. Exciton photophysics of carbon nanotubes. *Annu. Rev. Phys. Chem.* **2007**, *58*, 719–747.

40 Ma, Y. Z; Valkunas, L.; Dexheimer, S. L.; Bachilo, S. M.; Fleming, G. R. Femtosecond spectroscopy of optical excitations in single-walled carbon nanotubes: Evidence for exciton-exciton annihilation. *Phys. Rev. Lett.* **2005**, *94*, No. 157402.

41 Matsunaga, R.; Matsuda, K.; Kanemitsu, Y. Evidence for dark excitons in a single carbon nanotube due to the Aharonov-Bohm effect. *Phys. Rev. Lett.* **2008**, *101*, No. 147404.

42 Matsuda, K.; Inoue, T.; Murakami, Y.; Maruyama, S.; Kanemitsu, Y. Exciton dephasing and multiexciton recombinations in a single carbon nanotube. *Phys. Rev. B.* **2008**, *77*, No. 033406.

43 Ueda, A.; Matsuda, K.; Tayagaki, T.; Kanemitsu, Y. Carrier multiplication in carbon nanotubes studied by femtosecond pump-probe spectroscopy. *Appl. Phys. Lett.* **2008**, *92*, No. 233105.

44 Wang, S.; Khafizov, M.; Tu, X.; Zheng, M.; Krauss, T. D. Multiple exciton generation in single-walled carbon nanotubes. *Nano Lett.* **2010**, *10*, 2381–2386.

45 Ando, T. Effects of valley mixing and exchange on excitons in carbon nanotubes with Aharonov-Bohm flux. *J. Phys. Soc. Jpn.* **2006**, *75*, No. 024707.

46 Matsunaga, R.; Matsuda, K.; Kanemitsu, Y. Observation of charged excitons in hole-doped carbon nanotubes using photoluminescence and absorption spectroscopy. *Phys. Rev. Lett.* **2011**, *106*, No. 037404.

47 Nishihara, T.; Yamada, Y.; Kanemitsu, Y. Dynamics of exciton-hole recombination in hole-doped single-walled carbon nanotubes. *Phys. Rev. B* **2012**, *86*, No. 075449.

48 Klimov, V. I.; McGuire, J. A.; Schaller, R. D.; Rupasov, V. I. Scaling of multiexciton lifetimes in semiconductor nanocrystals. *Phys. Rev. B* **2008**, *77*, No. 195324.

49 Ueda, A.; Tayagaki, T.; Kanemitsu, Y. Dynamics of quantized Auger recombination in CdSe nanocrystals studied by femtosecond intraband pump-probe spectroscopy. *J. Phys. Soc. Jpn.* **2009**, *78*, No. 083706.

50 Nirmal, M.; Dabbousi, B. O.; Bawendi, M. G.; Macklin, J. J.; Trautman, J. K.; Harris, T. D.; Brus, L. E. Fluorescence intermittency in single cadmium selenide nanocrystals. *Nature* **1996**, *383*, 802–804.

51 Efros, Al. L.; Rosen, M. Random telegraph signal in the photoluminescence intensity of a single quantum dot. *Phys. Rev. Lett.* **1997**, *78*, 1110–1113.

52 Galland, C.; Ghosh, Y.; Steinbruck, A.; Sykora, M.; Hollingsworth, J. A.; Klimov, V. I.; Htoon, H. Two types of luminescence blinking revealed by spectroelectrochemistry of single quantum dots. *Nature* **2011**, *479*, 203–207.

53 Taguchi, S.; Ishizumi, A.; Kanemitsu, Y. Multicarrier recombination and energy transfer in Mn-doped CdS nanocrystals studied by femtosecond pump-probe spectroscopy. *J. Phys. Soc. Jpn.* **2010**, *79*, No. 063710.

54 White, M. A.; Weaver, A. L.; Beaulac, R.; Gamelin, D. R. Electrochemically controlled Auger quenching of Mn^{2+} photoluminescence in doped semiconductor nanocrystals. *ACS Nano* **2011**, *5*, 4158–4168.

55 Kobayashi, Y.; Nishimura, T.; Yamaguchi, H.; Tamai, N. Effect of surface defects on Auger recombination in colloidal CdS quantum dots. *J. Phys. Chem. Lett.* **2011**, *2*, 1051–1055.

56 Ueda, K.; Tayagaki, T.; Fukuda, M.; Fujii, M.; Kanemitsu, Y. Breakdown of the k-conservation rule in quantized Auger recombination in $Si_{1-x}Ge_x$ nanocrystals. *Phys. Rev. B* **2012**, *86*, No. 155316.

57 Pietryga, J. M.; Zhuravlev, K. K.; Whitehead, M.; Klimov, V. I.; Schaller, R. D. Evidence for barrierless Auger recombination in PbSe nanocrystals: A pressure-dependent study of transient optical absorption. *Phys. Rev. Lett.* **2008**, *101*, No. 217401.

58 Kanemitsu, Y. Light emission from silicon nanoparticles and related materials. In *Comprehensive Semiconductor Science and Technology*; Bhattacharya, P., Fornari, R., Kamimura, H., Eds.; Elsevier: Amsterdam, 2011; Vol. 2, pp 196−212.

59 Kovalev, D.; Heckler, H.; Polisski, G.; Koch, F. Optical properties of Si nanocrystals. *Phys. Status Solidi B* **1999**, *215*, 871–932.

60 Kanemitsu, Y.; Okamoto, S. Phonon structures and Stokes shift in resonantly excited luminescence of silicon nanocrystals. *Phys. Rev. B* **1998**, *58*, 9652–9655.

61 Hybertsen, M. S. Absorption and emission of light in nanoscale silicon structures. *Phys. Rev. Lett.* **1994**, *72*, 1514–1517.

62 Svantesson, K. G; Nilsson, N. G. The temperature dependence of the Auger recombination coefficient of undoped silicon. *J. Phys. C* **1979**, *12*, 5111–5120.

63 Beard, M. C.; Knutsen, K. P.; Yu, P.; Luther, J. M.; Song, Q.; Metzger, W. K.; Ellingson, R. J.; Nozik, A. J. Multiple exciton generation in colloidal silicon nanocrystals. *Nano Lett.* **2007**, *7*, 2506–2512.

64 Saruyama, M.; So, Y. G.; Kimoto, K.; Taguchi, S.; Kanemitsu, Y.; Teranishi, T. Spontaneous formation of wurtzite-CdS/zinc blende-CdTe heterodimers through a partial anion exchange reaction. *J. Am. Chem. Soc.* **2011**, *133*, 17598–17601.

65 Beard, M. C.; Midgett, A. G.; Law, M.; Semonin, O. E.; Ellingson, R. J.; Nozik, A. J. Variations in the quantum efficiency of multiple exciton generation for a series of chemically treated PbSe nanocrystal films. *Nano Lett.* **2009**, *9*, 836–845.

66 Tisdale, W. A.; Williams, K. J.; Timp, B. A.; Norris, D. J.; Aydil, E. S.; Zhu, X.-Y. Hot-electron transfer from semiconductor nanocrystals. *Science* **2010**, *328*, 1543–1547.

67 Hosoki, K.; Tayagaki, T.; Yamamoto, S.; Matsuda, K.; Kanemitsu, Y. Direct and stepwise energy transfer from excitons to plasmons in close-packed metal and semiconductor nanoparticle monolayer films. *Phys. Rev. Lett.* **2008**, *100*, No. 207404.